JACS
JOURNAL OF THE AMERICAN CHEMICAL SOCIETY
pubs.acs.org/JACS
Article

Rare-Earth Supported Nickel Catalysts for Alkyne Semihydrogenation: Chemo- and Regioselectivity Impacted by the Lewis Acidity and Size of the Support

Bianca L. Ramirez and Connie C. Lu*

Cite This: J. Am. Chem. Soc. 2020, 142, 5396−5407
Read Online

ABSTRACT: Bimetallic catalysts of nickel(0) with a trivalent rare-earth ion or Ga(III), $NiML_3$ (where L is $[^iPr_2PCH_2NPh]^-$, and M is Sc, Y, La, Lu, or Ga), were investigated for the selective hydrogenation of diphenylacetylene (DPA) to (*E*)-stilbene. Each bimetallic complex features a relatively short Ni−M bond length, ranging from 2.3395(8) Å (Ni−Ga) to 2.5732(4) Å (Ni−La). The anodic peak potentials of the $NiML_3$ complexes vary from −0.48 V to −1.23 V, where the potentials are negatively correlated with the Lewis acidity of the M(III) ion. Three catalysts, Ni−Y, Ni−Lu, and Ni−Ga, showed nearly quantitative conversions in the semihydrogenation of DPA, with $NiYL_3$ giving the highest selectivity for (*E*)-stilbene. Initial rate studies were performed on the two tandem catalytic reactions: DPA hydrogenation and (*Z*)-stilbene isomerization. The catalytic activity in DPA hydrogenation follows the order Ni−Ga > Ni−La > Ni−Y > Ni−Lu > Ni−Sc. The ranking of catalysts by (*Z*)-stilbene isomerization initial rates is Ni−Ga ≫ Ni−Sc > Ni−Lu > Ni−Y > Ni−La. *In operando* ^{31}P and ^1H NMR studies revealed that in the presence of DPA, the Ni bimetallic complexes supported by Y, Lu, and La form the Ni(η^2-alkyne) intermediate, (η^2-PhC≡CPh)Ni($^iPr_2PCH_2NPh$)$_2$M-(κ^2-$^iPr_2PCH_2NPh$). In contrast, the Ni−Ga resting state is the Ni(η^2-H_2) species, and Ni−Sc showed no detectable binding of either substrate. Hence, the mechanism of Ni-catalyzed diphenylacetylene semihydrogenation adheres to two different kinetics: an autotandem pathway (Ni−Ga, Ni−Sc) versus temporally separated tandem reactions (Ni−Y, Ni−Lu, Ni−La). Collectively, the experimental results demonstrate that modulating a base-metal center via a covalently appended Lewis acidic support is viable for promoting selective alkyne semihydrogenation.

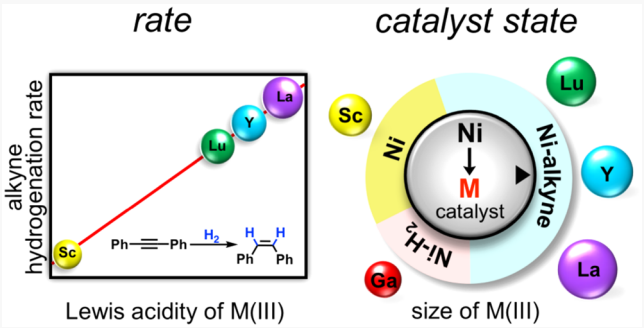

INTRODUCTION

The recent emergence of coordination compounds containing metal−metal bonds between transition metals (TMs) and rare earth (RE) elements, that is, the group 3 metals and the lanthanides (Ln), has inspired their use in diverse applications.[1−14] For example, TM−RE bonded complexes are currently being explored for single-molecule magnetism.[15,16] In the realm of catalysis, multimetallic cooperativity between rare earth ions and transition metals can elicit beneficial activity in both heterogeneous[17,18] and cluster[19−22] systems by affecting the catalyst stability, electronics, and/or substrate binding affinity. Even so, direct TM−RE bonds, especially those involving lanthanides, are rarely seen in homogeneous catalysis. Relevant precedents are the rare-earth complexes supported by ferrocene diamide ligands that catalyze ring-opening polymerization, wherein a weak metal−metal interaction was proposed to influence catalytic activity.[23−25] Fueled by the rise of bifunctional transition-metal catalysts with an appended Lewis acidic main group or Group 4 metal ion,[26−40] the extension to rare earth metals seemed ripe for exploration.

Our interest in using rare earth ions as a Lewis acidic support for tuning base metal reactivity was realized with the discovery of the catalytically active Ni−Lu complex, NiLu-($^iPr_2PCH_2NPh$)$_3$ (**1**). We demonstrated that the Lu(III) promotes Ni(0) activity in olefin hydrogenation. We also showed that the least coordinated (4-coordinate) Lu center, which gave the shortest Ni−Lu bond, also gave the fastest catalytic rates.[41] Because this work was the first example of a directly bound lanthanide ion being used as promoter for molecular base-metal catalysis, we became interested in exploring the catalytic reactivity of other nickel rare-earth bimetallic complexes and also turned our attention to the semihydrogenation of alkynes.

Received: January 23, 2020
Published: February 24, 2020

https://dx.doi.org/10.1021/jacs.0c00905
J. Am. Chem. Soc. 2020, 142, 5396−5407

The semihydrogenation of alkynes to alkenes is an industrially important transformation in bulk and fine chemical manufacturing.[42,43] However, due to the competitive formation of both (*E*)- and (*Z*)-isomers, as well as the overhydrogenated byproduct, the main challenge is to fully control both the chemo- and stereoselectivity of this reaction.[44] Classic alkyne semihydrogenation catalysts, such as Lindlar's catalyst[45] or the Schrock–Osborn catalyst,[46] can produce (*Z*)-alkenes efficiently, though careful control of reaction conditions is sometimes necessary to avoid overhydrogenation. The stereocomplementary formation of (*E*)-alkenes using H_2 as a reductant is significantly more challenging. As such, well-defined semihydrogenation catalysts that operate under an atmosphere of H_2 are surprisingly limited in number.[46−51]

With rare exceptions,[52−56] (*E*)-alkenes are most commonly formed via an initial hydrogenation of the alkyne to the (*Z*)-alkene, followed by *cis*-to-*trans*-alkene isomerization.[57−64] Within a broader catalytic context, the employment of nonprecious metal catalysts has attracted intense interest, not only for their affordability and sustainability, but also for their potential to provide unprecedented reactivity and/or selectivity.[65,66] Several (*E*)-selective semihydrogenation catalysts based on Co and Fe have been reported, but common drawbacks include limited substrate scope, the need for a high operating temperature, and/or lack of overall selectivity.[57−59,63] Recently, the first example of Ni-mediated semihydrogenation using H_2 as a reductant was reported using a mixture of $Ni(NO_3)_2{\cdot}6H_2O$ and triphos.[60] However, forcing reaction conditions (120 °C, 30 bar) were needed to achieve high yields and selectivity.

In this work, we have synthesized and structurally isolated an isostructural series of Ni(0)–RE(III) complexes, NiRE(^{i}Pr$_2$PCH$_2$NPh)$_3$ (where RE is Sc, Y, and La). In conjunction with the previously reported Ni–Lu complex (**1**), and NiGa(^{i}Pr$_2$PCH$_2$NPh)$_3$ for comparison with a nonrare earth support, the catalytic utility of the Ni bimetallic complexes toward the (*E*)-selective semihydrogenation of internal alkynes using H_2 at moderate pressure and temperature is presented.

RESULTS

Synthesis and Characterization of ML_3 and $NiML_3$. Scheme 1 illustrates the two synthetic routes used to prepare the $NiML_3$ series, where L is $[^i$Pr$_2$PCH$_2$NPh$]^-$. In the first route, the rare-earth metalloligands were isolated prior to metalation with Ni(0). The metalloligands, ScL_3 (**2**) and YL_3 (**3**), were obtained as white powders in good yields (85% and 88% yields, respectively) from the reaction of the corresponding MCl_3 (M = Sc or Y) and 3 equiv of the deprotonated ligand, Li[^{i}Pr$_2$PCH$_2$NPh]. The La(III) metalloligand, LaL_3 (**4**), was obtained from the reaction of La[N(TMS)$_2$]$_3$ and 3 equiv of ^{i}Pr$_2$PCH$_2$NHPh in 70% yield. In the second synthetic approach, the metalation sequence was flipped by installing the Ni(0) center first. From the reaction of 3 equiv of Li[^{i}Pr$_2$PCH$_2$NPh] with Ni(COD)$_2$, where COD = 1,5-cyclooctadiene, the Ni(0) complex, Ni(Li·L)$_3$ (**5**), was isolated as a purple solid (90% yield). For complexes **2**, **4**, and **5**, the corresponding ^{31}P{^{1}H} NMR spectra each display a singlet at −18.8, −12.6, and 20.1 ppm, respectively (Figure S1). The ^{31}P NMR spectrum of **3** shows a doublet at −14.1 ppm with a coupling constant (J_{P-Y}) of 36.5 Hz to the I = 1/2 ^{89}Y nucleus. The ^{1}H{^{31}P} NMR spectrum of **2** has 10 peaks, which is consistent with C_3 symmetry: 3 aryl protons, 2 diastereotopic methylene protons, 2 unique methine protons, and 3 methyl

Scheme 1. Synthetic Pathways of Heterobimetallic $NiML_3$ Complexes 6–9, where M = Sc, Y, La, and Ga

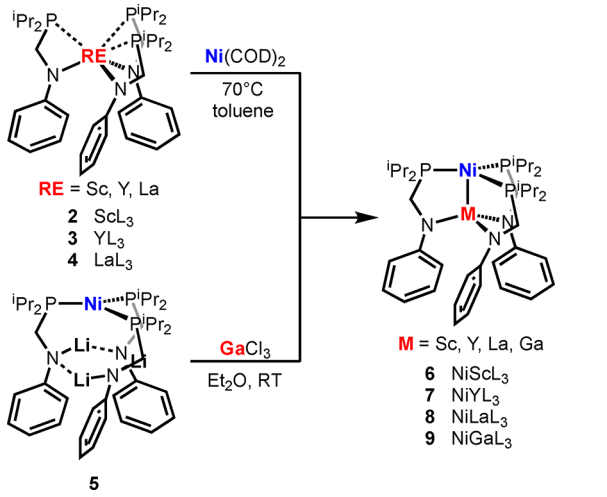

peaks that integrate to 18H, 9H, and 9H. The 2:1:1 integration ratio supports the assignment of P(CHMe$_2$)(CHMe′Me″), where one of the two ^{i}Pr substituents displays hindered P–C bond rotation (Figure S4). On the other hand, the ^{1}H{^{31}P} NMR spectra of **3**, **4**, and **5** each display a singlet for the methylene protons. These complexes are presumably more fluxional, such that the averaged solution structure exhibits C_{3v} symmetry (Figures S6, S8, and S10).

The heterobimetallic complexes $NiScL_3$ (**6**), $NiYL_3$ (**7**), and $NiLaL_3$ (**8**) were isolated as bright red to orange crystals from the reaction of Ni(COD)$_2$ with **2**, **3**, and **4**, respectively (crystalline yields 72 to 80%). Further, addition of $GaCl_3$ to **5** afforded $NiGaL_3$ (**9**) after workup as a brown solid (60% yield). The NMR spectra of all these $NiML_3$ compounds display a single ^{31}P{^{1}H} resonance and a single ^{1}H{^{31}P} resonance for the methylene protons, consistent with C_{3v} symmetry in solution (Figures S12–S15, S18, S19, and S21). Of note, the ^{31}P{^{1}H} NMR shifts in aromatic solvents for the Ni–rare earth series vary subtly (range: −0.8 ppm for **1** to 3.1 ppm for **6**, Figure S12), whereas the resonance of Ni–Ga **9** appears significantly more downfield at 31.8 ppm.

Previously, we noted that adding THF to a toluene-d_8 solution of $NiLuL_3$ (**1**) generated an equilibrium mixture of **1** and **1**–THF, in which a single molecule of THF binds to the Lu center.[41] Complete THF binding resulted in a significant 11-ppm downfield shift of the ^{31}P NMR resonance. Herein, a similar behavior was observed for **7** ($\Delta(^{31}P\ \delta)$ = +8 ppm) and to a smaller extent for **8** ($\Delta(^{31}P\ \delta)$ = +2.5 ppm at rt, +6.6 ppm at −83 °C), suggesting that **7**–THF and **8**–THF are accessible (Figures S13 and S101). By comparison, the change in the ^{31}P δ for **6** or **9** is negligible when dissolved in THF-d_8 versus that in toluene-d_8 ($\Delta(^{31}P\ \delta) < 0.3$ ppm). These findings indicate that THF binding to a $NiML_3$ complex can be controlled by the size of M, where a sufficiently large M center (Lu, Y, and La) allows the solvent to bind.

To probe the impact of the M(III) supports on the electronics at Ni, a cyclic voltammetry (CV) study of the $NiML_3$ series was performed. The cyclic voltammograms were collected at 100 mV/s in 0.1 M [^{n}Pr$_4$N][BAr$^F_4$]/1,2-difluorobenzene electrolyte solutions (where Ar^F is 3,5-bis(trifluoromethyl)phenyl) and internally referenced to the $[FeCp_2]^{+/0}$ potential. Each $NiML_3$ complex showed an

https://dx.doi.org/10.1021/jacs.0c00905
J. Am. Chem. Soc. 2020, 142, 5396−5407

irreversible Ni(I/0) oxidation process, with the anodic peak potential (E_{pa}) shifting overall by 0.75 V (Figure S27). The E_{pa} values increase in the order −1.23 V (for **7**) < −1.17 V (**8**) < −1.00 V (**1**)[41] < −0.57 V (**6**) < −0.48 V (**9**). The Ni(I/0) peak potentials in this $NiML_3$ series correlate well with the Lewis acidity of the M(III) ion, which is parametrized by the pK_a values of the aquo species $[M(OH_2)_6]^{3+}$ (R^2_{adj} = 0.91, Table S3, Figure S29).[67−70] This is in accord with the rationale that more Lewis acidic M(III) ions will withdraw electron density from Ni to a greater extent, which leads to more positive Ni(I/0) peak potentials. Of interest to us, the peak potentials showed a worse correlation with size of the M(III) ion using the Shannon M(III) ionic radii (R^2_{adj} = 0.77, Table S3),[39,71] which suggests that the flexible nature of L does not accentuate size effects of the M(III) support on the Ni electronics.[38]

X-ray Crystallography. Single-crystal X-ray diffraction studies were conducted on all monometallic and bimetallic compounds. The solid-state structures and geometrical parameters for monometallic **2**−**5** are provided in the SI (Figures S30−S33, Table S4). The solid-state structures of the bimetallic Ni−M complexes **6**−**9** are shown in Figure 1, with

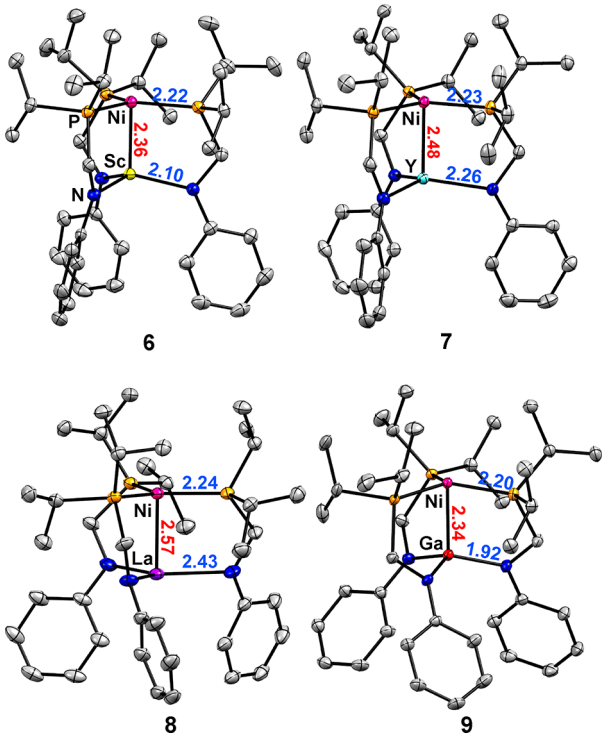

Figure 1. Molecular structures of **6**−**9** shown at 50% thermal ellipsoid probability. Hydrogen atoms and lattice solvent molecules have been omitted for clarity. The average bond lengths (Å) are shown. Atom colors: Sc, yellow; Y, light blue; La, purple; Ga, red; Ni, pink; P, orange; N, blue; C, gray.

selected bond distances and other geometrical parameters in Table 1. The $NiML_3$ complexes are all isostructural and possess approximate C_3 symmetry. By examining the structures of **1** and **6**−**9**, the impact of M on various bond lengths was assessed. Of note, the Shannon ionic radii of the M(III) ions vary by 0.41 Å, with Ga(III) possessing the smallest ionic radius (0.620 Å) and La(III) possessing the largest (1.032 Å).[72] Both the M−N and Ni−M bonds in **1** and **6**−**9** adhere to the same trend: these bonds elongate according to M = Ga < Sc < Lu < Y < La. This accords well with the expected trend based on M(III) radii (Figures S36−S38, Table S7). In comparing Ni−Ga **9** and Ni−La **8**, which represent the two M(III) size extremes, the M−N and Ni−M bond distances differ by 0.51 and 0.23 Å, respectively. On the other hand, the Ni−P bond lengths do not substantially change (Δ = 0.03 Å).

The intermetal distances in **1** and **6**−**9** are all shorter than the sum of the two metals' covalent radii, signifying a significant Ni−M bonding interaction. To better compare the metal−metal interactions, we calculated the formal shortness ratio (r) or the ratio of the Ni−M bond distance to the sum of their respective covalent radii using Pyykkö covalent radii values.[73] The r values across the rare-earth supported bimetallic complexes are all similar, 0.89 to 0.91. This suggests that the bonding interaction between Ni and the rare earth ion is independent of the rare earth identity. We further note that the similar r values are not simply a consequence of the bridging ligand L since Ni−Ga **9** has a significantly larger r value of 1.00.

Catalyst Screening for Diphenylacetylene Semihydrogenation. The effect of varying the Lewis acid support on both catalytic activity and selectivity was investigated using the semihydrogenation of diphenylacetylene (DPA) as a model reaction (Table 2, Figures S39−S46). In a standard catalytic run, a J Young NMR tube loaded with the catalyst (2.5 mol %) and substrate (0.45 M DPA) in toluene-d_8 was charged with 4 atm of H_2 and heated to 70 °C for 24 h (4.6 atm H_2 at 70 °C). A mixture of $Ni(COD)_2$ and 3 equiv of the protioligand was tested as a control for a monometallic nickel catalyst (entry 1). This catalyst system gave poor DPA conversion (<40%). In addition, alkyne semihydrogenation proceeded nonselectively to a ∼1:1 mixture of (*E*)- and (*Z*)-stilbene with a small amount (6%) of the double alkyne insertion byproduct, 1,2,3,4-tetraphenyl-1,3-butadiene, which will simply be referred to as the (*Z*,*Z*)-diene. Mononickel complex **5** performed similarly poorly (entry 2). The catalytic performance of bimetallic **1** and **6**−**9** are shown in entries 3−7. With the single exception of Ni−Sc **6**, all the Ni−M catalysts showed nearly complete DPA conversion (≥98%) under the standard catalytic conditions. The best performer was Ni−Y **7**, which quantitatively converted DPA to (*E*)-stilbene (entry 5). Both Ni−Lu **1** and Ni−Ga **9** generated (*E*)-stilbene in high yields (91%); however, both catalysts also generated a significant amount (7−9% yield) of the undesired byproducts: 1,2-diphenylethane, which results from double hydrogenation, and (*Z*,*Z*)-diene.

Unexpectedly, Ni−La **8** showed an inverted preference for (*Z*)-stilbene over the (*E*)-isomer by a factor of 4. We note, however, that during the catalysis time course of **8**, we observed the gradual growth of different decomposition species, including $^{i}Pr_2PH$. Hence, a more reasonable explanation is that the *cis*-to-*trans* stilbene isomerization was impeded by catalyst death. In support, all $NiML_3$ complexes, including **8**, catalyze the isomerization of (*Z*)-stilbene to (*E*)-stilbene under the standard catalytic conditions (SI Table S10). Among the bimetallic catalysts, Ni−Sc **6** performed the worst, as it reacted sluggishly and produced the most (*Z*,*Z*)-diene byproduct (15%).

The choice of solvent was found to be critical for the high catalytic selectivity of **7**. Upon changing the solvent to THF-d_8, the performance of catalyst **7**, as the THF adduct **7**−THF, suffered greatly, as evidenced by marked decline in both

https://dx.doi.org/10.1021/jacs.0c00905
J. Am. Chem. Soc. 2020, 142, 5396−5407

Table 1. Geometrical Parameters, Including Bond Lengths (Å) and Angles (deg), for 6–9

	1	6	7	8	9[a]
M(III) ionic radius (Å)[b]	0.861 (Lu)	0.745 (Sc)	0.900 (Y)	1.032 (La)	0.620 (Ga)
pK_a of $[M(OH_2)_6]^{3+}$	7.90	5.11	8.43	9.06	2.95
Ni–M	2.4644(2)	2.3569(7)	2.4823(3)	2.5732(4)	2.3395(8)
r[c]	0.91	0.91	0.91	0.89	1.00
Ni–P[d]	2.2188(2)	2.2184(2)	2.2268(3)	2.2352(3)	2.2027(3)
M–N[d]	2.213(1)	2.102(1)	2.258(1)	2.429(1)	1.9181(1)
Σ P–Ni–P	359.40(1)	359.53(1)	359.75(4)	359.74(1)	357.57(3)
Σ N–M–N	352.39(8)	347.07(5)	354.81(10)	359.83(1)	345.74(6)
M to N_3 plane[e]	0.3559(7)	0.4427(15)	0.2994(10)	−0.06(6)	0.4243(5)
Ni to P_3 plane[f]	0.0995(3)	0.0881(6)	0.0645(4)	−0.07(2)	0.1991(2)

[a]Two molecules in the asymmetric unit. Values are averages. [b]Shannon ionic radius of six-coordinate M(III).[72] [c]Formal shortness ratio.[73] See the main text. [d]Average value. [e]Positive value indicates M is positioned closer to Ni. [f]Positive value indicates Ni is positioned away from M.

Table 2. Catalyst Screening for Semihydrogenation of Diphenylacetylene (DPA)[a,b]

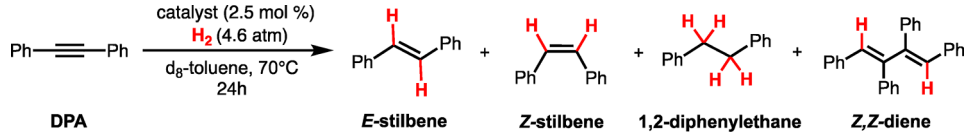

entry	catalyst	DPA conversion (%)	stilbene (%)	*E*:*Z* stilbene ratio	diphenylethane (%)	*Z*,*Z*-diene[c] (%)
1	$Ni(COD)_2$ + 3 HL	38	32	52:48	0	6
2	**5** $Ni(Li{\cdot}L)_3$	29	28	25:75	<1	<1
3	**1** (Lu)	>99	91	>99:1	7	2
4	**6** (Sc)	74	58	40:60	1	15
5	**7** (Y)	>99	99	>99:1	<1	<1
6	**8** (La)	98	91	20:80	2	5
7	**9** (Ga)	>99	92	>99:1	1	7
8[d]	7–THF-d_8	>99	78	40:60	21	<1
9[e]	7 + Hg^0	>99	99	>99:1	<1	<1

[a]Catalytic conditions: 2.5 mol % catalyst, 0.45 M DPA, ca. 500 μL of toluene-d_8, 4.6 atm H_2 at 70 °C, 24 h. [b]Values (%) are averages of triplicate runs and were determined by ^{1}H NMR integration using 1,3,5-trimethoxybenzene as an internal standard (error = ±0.5%). [c]*Z*,*Z*-Diene = 1,2,3,4-tetraphenyl-1,3-butadiene. [d]THF-d_8 solvent. [e]300 equiv of Hg metal.

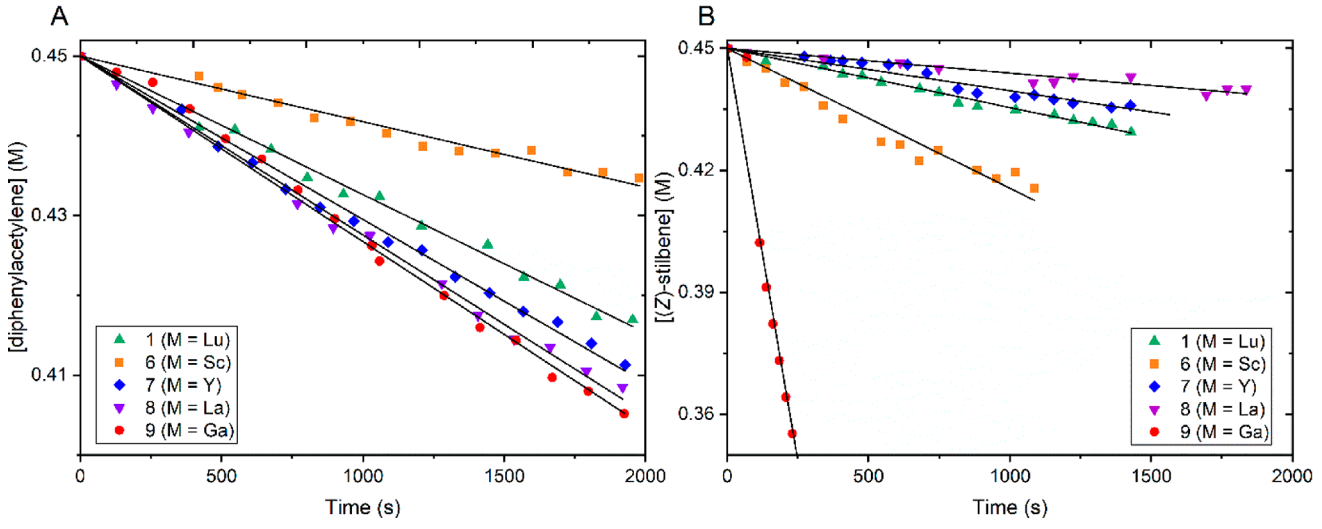

Figure 2. Kinetic plots of substrate concentration (M) versus initial time (s) for **A**) the hydrogenation of diphenylacetylene and **B**) isomerization of (*Z*)-stilbene, as catalyzed by **1** and **6**–**9** under the standard catalytic conditions. For more details, see SI Figures S47–S57.

regioselectivity (*E*:*Z*-stilbene ratio of 2:3) and chemoselectivity (alkyne versus alkene hydrogenation), as indicated by >20% yield of 1,2-diphenylethane (entry 8). Lastly, catalysis by **7** was uninhibited in the presence of excess Hg, which supports a homogeneous active species (entry 9).

Initial Rate Studies. The (*E*)-selective hydrogenation of disubstituted alkynes proceeds by an autotandem catalytic process, in which a single catalyst executes both the *syn*-hydrogenation of the alkyne and the *cis*-to-*trans* isomerization of the resulting alkene. To disentangle the two catalytic cycles,

https://dx.doi.org/10.1021/jacs.0c00905
J. Am. Chem. Soc. 2020, 142, 5396–5407

we separately conducted initial rate studies of DPA hydrogenation and (*Z*)-stilbene isomerization. While H_2 is not consumed in the latter reaction, H_2 was found to be necessary because alkene isomerization either does not proceed or is very sluggish in the absence of H_2 (Table S11). The initial rates were determined by monitoring the consumption of the starting material (DPA or (*Z*)-stilbene) under the standard catalytic conditions until either 10% conversion or up to 1 h. The kinetic plots are shown in Figure 2, and the initial rates are listed in Table 3. Of note, catalyst **8** did not decompose during this short time period.

Table 3. Initial Rate Data for the *Syn*-Hydrogenation of DPA and (*Z*)-to-(*E*) Stilbene Isomerization by $NiML_3$ Catalysts[a]

		initial rate ($\times 10^{-5}$ M/s)	
entry	catalyst	$-$d[DPA]/dt[b]	$-$d[(*Z*)-stilbene]/dt
1	**1** (Lu)	1.71(8)	1.4(1)
2	**6** (Sc)	0.67(4)[c]	3.0(2)
3	**7** (Y)	1.9(4)	1.1(1)
4	**8** (La)	2.13(1)	0.45(3)
5	**9** (Ga)	2.5(4)	40.4(7)

[a]Catalytic conditions: 2.5 mol % catalyst, 0.45 M DPA, or (*Z*)-stilbene, ca. 500 μL of toluene-d_8, 4.6 atm H_2 at 70 °C, ≤1 h with an internal standard of 1,3,5-trimethoxybenzene (0.02 mmol). [b]In all cases except **6**, (*Z*)-stilbene was formed cleanly in the *syn*-hydrogenation, and the rate of the reaction is $-$d[DPA]/dt. [c]For **6**, formation of both (*Z*,*Z*)-diene and (*E*)-stilbene were observed, and the corrected rate of *syn*-hydrogenation = $-$d[DPA]/dt $-$ d[*Z*,*Z*-diene]/dt. See the SI for details.

In both reactions, Ni−Ga **9** was the fastest of the $NiML_3$ catalysts. Changing the metal support impacted the catalytic activity, especially in the (*Z*)-stilbene isomerization reaction, where the initial rates varied by nearly 90-fold. On the other hand, the initial rates for DPA hydrogenation only varied by a factor of 3. With the exception of Ni−Ga **9**, the two reactions showed opposite trends in catalytic activity for the different metal supports. For example, catalytic activity in DPA hydrogenation follows the order **9** (M = Ga) > **8** (La) > **7** (Y) > **1** (Lu) > **6** (Sc). By comparison, the ranking of catalysts by (*Z*)-stilbene isomerization activity is **9** (M = Ga) ≫ **6** (Sc) > **1** (Lu) > **7** (Y) > **8** (La). Upon excluding **9**, a *positive* correlation was found between the rate of DPA hydrogenation and the pK_a value of the corresponding aquo species $[M(OH_2)_6]^{3+}$ (Figure 3, slope = $+0.37(1) \times 10^{-5}$ M/s per pK_a unit; R^2_{adj} = 0.99). This finding suggests that *less* Lewis acidic supports result in greater Ni-based activity in alkyne *syn*-hydrogenation (Figure S58). As an aside, a reasonable correlation also exists between the rate of DPA hydrogenation and E_{pa} for the Ni-rare earth catalysts (R^2_{adj} = 0.94, Table S8). Also excluding **9**, the plot of the (*Z*)-stilbene isomerization rate versus the pK_a value of $[M(OH_2)_6]^{3+}$ showed a *negative* correlation (Figure 3, slope = $-0.62(5) \times 10^{-5}$ M/s per pK_a unit; R^2_{adj} = 0.98), indicating that *more* Lewis acidic supports lead to higher activity in *cis*-to-*trans* alkene isomerization (Figure S59). However, for both reactions, the initial rates for **9** are significantly faster than the correlative values based on Lewis acidity (Figures S60 and S61), suggesting the Ga^{III} supporting ion, which is by far the most Lewis acidic, results in a significant change in the nature of the reactive species and/or the mechanism.

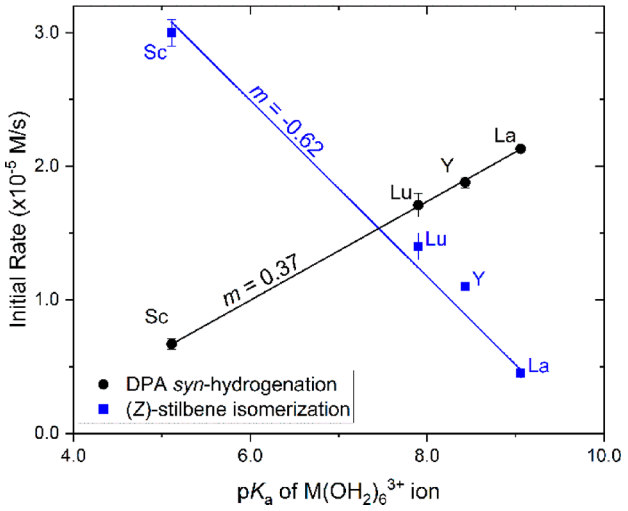

Figure 3. Plot of the initial rate of *syn*-hydrogenation of diphenylacetylene (black circles, R^2_{adj} = 0.99) and *cis*-to-*trans* isomerization of (*Z*)-stilbene (blue squares, R^2_{adj} = 0.98) versus pK_a of $M(OH_2)_6^{3+}$ for catalysts **1** and **6**−**8**. The slope, *m*, is provided in the plots.

***In Operando* Catalytic Studies.** To further investigate the impact of the supporting metal, the full reaction time course from DPA to (*E*)-stilbene was monitored by ^{1}H NMR spectroscopy under the standard catalytic conditions. Three catalysts, Ni−Ga **9**, Ni−Sc **6**, and Ni−Y **7**, were selected because they exhibit markedly different rates and/or selectivity. In the reaction catalyzed by Ni−Ga **9** (Figure 4A), (*Z*)-stilbene is the first intermediate to accumulate, reaching maximum concentration at ∼4.5 h, before fully decaying as it converts to (*E*)-stilbene within 8 h. By comparison, the Ni−Sc **6** catalyst required a significantly longer time period (70 h) for the reaction to fully consume (*Z*)-stilbene (Figure 4B). In addition to the (*E*)-stilbene product, the (*Z*,*Z*)-diene by-product was formed in significant amounts and primarily at early reaction times when DPA is present. This suggests that after DPA insertion into a Ni−H bond to form a Ni−vinyl intermediate, an off-pathway insertion of a second DPA is competitive with the on-pathway reductive elimination of (*Z*)-stilbene.

The reaction time course for Ni−Y **7** was remarkably distinct in that a temporal separation of the two catalytic reactions was clearly observed. The *cis*-to-*trans* isomerization of stilbene proceeded only *after* the DPA was almost entirely consumed in the *syn*-hydrogenation reaction (Figure 4C). Temporal separation in autotandem catalysis is rare. To our knowledge, the single well-studied precedent,[Ru(Cp)(bpy)(NCMe)]$^+$, converts terminal alkynes into the corresponding alcohols through an acetaldehyde intermediate.[74] The temporal separation of the two catalytic cycles also indicates a greater chemoselectivity for DPA relative to (*Z*)-stilbene by **7**. Also of relevance, strong alkyne adsorption and its impact on kinetics had been observed for Cu/SiO_2, a heterogeneous catalyst for (*Z*)-selective semihydrogenation.[75] Lastly, we note that during the reaction time course shown in Figure 4C, the rate of stilbene isomerization exceeded that of DPA hydrogenation. This was unexpected because the initial rate studies showed the opposite order, where DPA hydrogenation was 1.7 times faster than that of stilbene isomerization. We do not currently understand the origin of the rate enhancement, but

https://dx.doi.org/10.1021/jacs.0c00905
J. Am. Chem. Soc. 2020, 142, 5396−5407

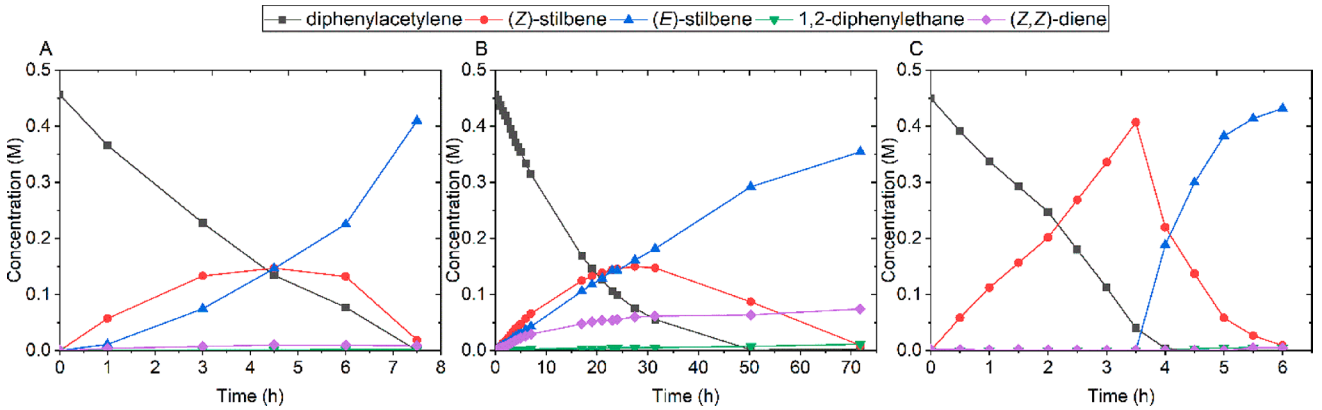

Figure 4. Reaction time course for the semihydrogenation of diphenylacetylene to (*E*)-stilbene under standard conditions for catalysts: A) Ni−Ga **9**, B) Ni−Sc **6**, and C) Ni−Y **7**.

we speculate that small amounts of DPA might alter the catalyst speciation to a more reactive species for stilbene isomerization (Figure S76).

Catalyst Resting State. The reaction time course experiments were also monitored by $^{31}P\{^{1}H\}$ NMR spectroscopy to elucidate the catalyst resting state. Throughout the full reaction time course, the catalytic reaction mixture of Ni−Sc **6** only showed the presence of **6** (Figure S66). Hence, no observable binding of either H_2 or DPA was found for the Sc(III)-supported Ni site. During the *in operando* catalysis by Ni−Ga **9**, a single complex with a corresponding $^{31}P\{^{1}H\}$ NMR singlet at 48.5 ppm was observed throughout the full time course (Figures S72 and S78). This new species also exhibited a broad ^{1}H NMR resonance at −2.03 ppm, which is typical of a Ni(η^2-H_2) adduct (Figure S85).[76,77] Also, consistent with H_2 binding, the reaction solution color bleached from a dark red-orange (**9**) to a light yellow-orange (**9**−H_2).[71] Hence, the strongly Lewis acidic Ga(III) ion promotes H_2 binding at the supported Ni site. Further characterization of the independently synthesized **9**−H_2 includes a T_1(min) value of 28(1) ms (500 Hz), which confirms an intact H−H bond (Figure S86).[76] An H−H distance of 0.86 Å (cf. 0.74 Å in free H_2) was determined from the J_{H-D} value of 35 Hz for the corresponding HD adduct (Figure S87).[77] H_2 binding was reversible as evacuating a solution of **9**−H_2 regenerates **9**. Of note, the H_2 binding behavior of **9** contrasts that of Ni−Lu **1**, where H_2 binding is so weak that it was only perceptible at the low temperature of −80 °C and under 4 atm H_2. The other rare-earth supported Ni complexes herein also show similarly weak H_2 binding akin to **1** (Figures S88−S102).

The *in operando* catalysis of **7** also showed complete formation of a new species that persisted until t ∼3.5 h. After t ∼3.5 h, the only species observed was **7**. The $^{31}P\{^{1}H\}$ NMR spectrum of this new complex consists of a singlet resonance at 30.4 ppm and a doublet at −11.5 ppm (J = 48.4 Hz), with an integration ratio of 2:1, respectively (Figure S68). The observed coupling makes evident that one phosphine donor is coordinated to ^{89}Y (>99% abundance, I = 1/2). We further infer that this ligand hemilability allows for strong alkyne binding at Ni. In support, identical spectroscopic features were observed when 5 equiv DPA was added to **7** (Figure S26). Structural elucidation of this species by single-crystal X-ray diffraction confirmed its assignment as the DPA adduct, (η^2-PhC≡CPh)Ni(^{i}Pr$_2$PCH$_2$NPh)$_2$Y(κ^2-^{i}Pr$_2$PCH$_2$NPh), or **7**−DPA (Figure 5). The favorable formation of **7**−DPA also rationalizes the greater chemoselectivity of **7** for DPA over stilbene, as well as the temporal separation of the two tandem reactions.

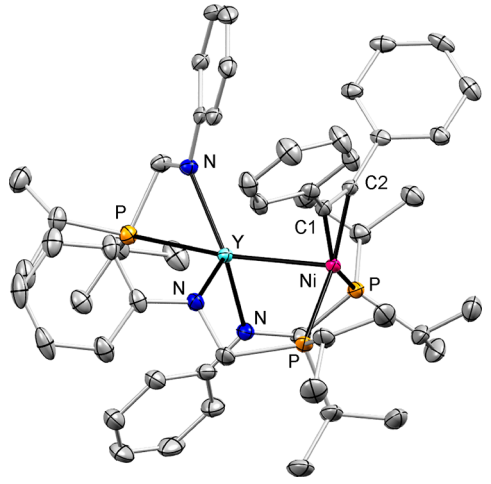

Figure 5. Molecular structure of **7**−DPA shown at 50% thermal ellipsoid probability; hydrogen atoms and noncoordinating solvent molecules are omitted for clarity. Only one of the two complexes from the asymmetric unit is shown for clarity. Selected interatomic distances (Å) and angles (deg) as an average of the two crystallized molecules in the asymmetric unit: Ni−Y, 2.7031(2); Y−P, 2.9896(5); C1−C2, 1.281(3); Ph−C1−C2, 142.5(2). See Table S6 for more details.

In the solid-state structure of **7**−DPA, two molecules crystallized in the asymmetric unit with an average Ni−Y bond length of 2.7031(2) Å, which is longer than that in **7** by 0.22 Å. The Ni−Y bonding interaction remains intact as suggested by the corresponding r value of 0.99. The average Y−P distance of 2.9896(5) Å is similar to those in the monometallic YL_3, **3**. Significant π-back-bonding into the alkyne is evidenced by the elongated C1−C2 distance (avg 1.281(3) Å) and the bent Ph−C1−C2 angle (avg 142.5(2)°). The geometric changes in the DPA ligand are similar to those in (η^2-PhC≡CPh)Co(^{i}Pr$_2$PNXyl)$_2$ZrI(THF), which is also a relevant intermediate in DPA semihydrogenation.[59] However, the regioselectivity of the Co−Zr catalyst is poor as stilbene was formed as a mixture of both the *cis* and *trans* isomers.[59] Lastly, the rearrangement of the [^{i}Pr$_2$PCH$_2$NPh]$^-$ ligand in **7**−DPA is reminiscent of the

https://dx.doi.org/10.1021/jacs.0c00905
J. Am. Chem. Soc. 2020, 142, 5396−5407

Table 4. Substrate Scope

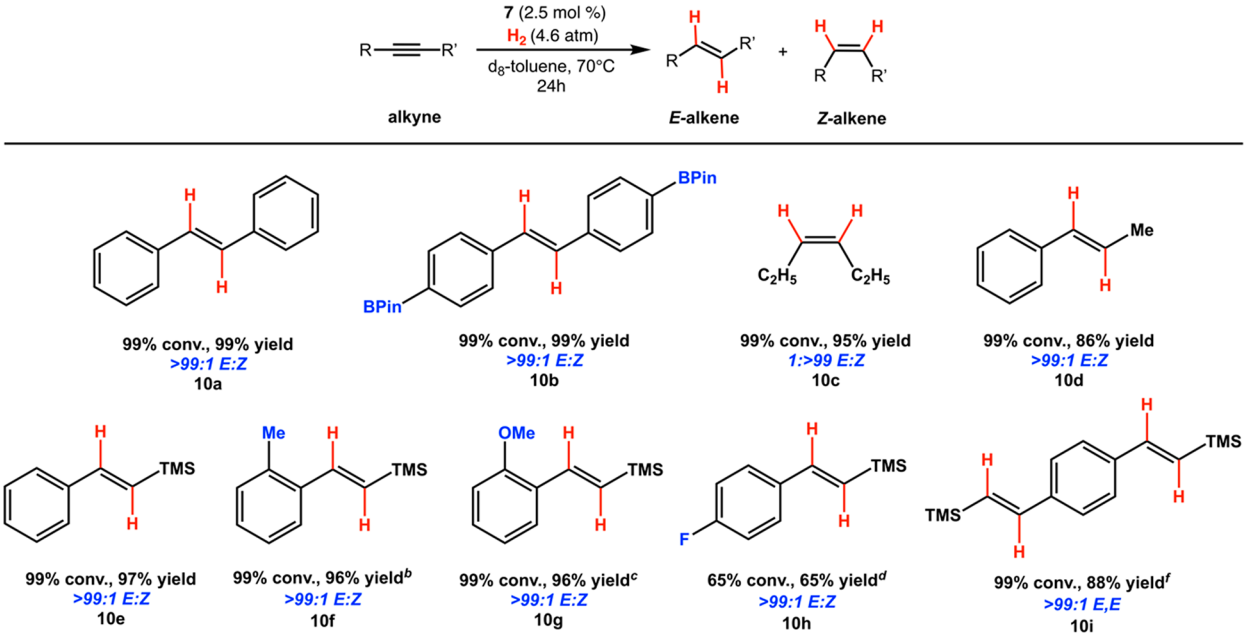

[a]Catalytic conditions: 2.5 mol % **7**, 0.45 M alkyne in ca. 500 μL of toluene-d_8, 4.6 atm H_2, heated to 70 °C, unless otherwise noted. Conversion is reported as an average of triplicate runs (±0.5% error bars) at 24 h (unless otherwise noted), as determined by ^{1}H NMR integration against an internal 1,3,5-trimethoxybenzene standard (0.02 mmol). [b]After 60 h. [c]3.5 mol % **7**. [d]5 mol % **7**, full catalyst decomposition after 24 h, remainder was alkyne. [e]After 48 h.

hemilability behavior observed in related heterobimetallic Co−Zr complexes bearing three bridging phosphinoamide ligands.[78,79]

The combination of ligand hemilability and DPA binding was also observed for Ni−Lu **1** and Ni−La **8** (Figure S62). Both catalysts **1** and **8** showed a clear temporal separation during catalysis, akin to **7**. These findings suggest that the strong alkyne chemoselectivity is linked to the M(III) rare-earth supports with sufficiently large ionic radii. Hence, we hypothesize that larger supporting metal ions enhance ligand hemilability, which then favors DPA binding. In support, neither Ni−Ga **9** nor Ni−Sc **6** showed any detectable binding of DPA even when DPA was present in large excess (40 equiv) or cooled to −60 °C (Figures S77−S78). To test whether a vacant coordination site at Y(III) in **7** is vital to its catalytic performance, we monitored the catalysis when the Y(III) center is saturated by a coordinating solvent molecule, such as THF. During the catalytic time course in THF, **7**−DPA was never observed (40 equiv of DPA). Instead, the only observed species was the THF adduct, **7**−THF, which was independently synthesized and crystallographically characterized (Figures S34 and S74, Table S6). The deterioration of the catalyst performance for **7**−THF suggests that having an open coordination site on Y to promote ligand hemilability may be critical to the enhanced performance of **7**.

Substrate Scope and Isotope-Labeling Studies. Encouraged by preliminary catalytic studies with DPA, we sought to investigate the utility of **7** toward the semihydrogenation of an assortment of substrates (Table 4, also see Figures S103−S111), using the standard catalytic conditions, unless otherwise noted. The *para*-substituted diarylacetylene featuring a boronate ester proceeded cleanly to the *trans*-diarylethene **10b** with excellent regioselectivity (>99:1 *E*:*Z*) and in 99% yield. 3-Hexyne, a dialkyl-substituted acetylene, gave nearly exclusively *cis*-3-hexene (**10c**) and some trace hexane. The clean formation of the *cis*-isomer suggests that dialkyl-substituted alkenes may not undergo the critical olefin insertion into the Ni−H species during the alkene-isomerization cycle (*vide infra*). Of interest, 1-phenylpropyne yielded the *trans*-alkene **10d** fairly cleanly. Terminal alkynes, on the other hand, are nonviable substrates. An attempted catalytic run with phenylacetylene resulted in catalyst decomposition and no hydrogenation product(s). If instead, the trimethylsilyl protecting group is employed, such as 1-phenyl-2-trimethylsilylacetylene, then the *trans*-alkene **10e** is formed nearly exclusively. Several 1-aryl-2-trimethylsilylacetylene substrates were also investigated, including methoxy or methyl *ortho*-substituted or *para*-substituted fluorine derivatives. For these substrates, the corresponding *trans* products (**10f**−**10h**) were obtained in good yields with excellent regioselectivity, though either higher catalyst loadings (up to 5 mol %) or longer reaction times (up to 60 h) were necessary. Lastly, a substrate bearing two internal alkynes reacted cleanly in a double semihydrogenation with excellent (*E*,*E*)-selectivity (**10i**).

As previously discussed, the alkene *cis*-to-*trans* isomerization does not consume H_2, but H_2 is required for the reaction to be kinetically relevant. An isotopic labeling experiment was performed using catalysts **7** and **9**. Using D_2 and otherwise standard catalytic conditions, (*Z*)-stilbene was converted to (*E*)-stilbene with deuterium incorporation. Also, formation of HD, and a minor amount of H_2, was observed for catalyst **7** (Figures S80−S81). A control experiment showed that **7** does not scramble HD to produce H_2 and D_2 under the same conditions. Hence, the origin of the protons in HD and H_2 is most likely the (*Z*)-stilbene substrate. This supports the alkene isomerization proceeding via alkene insertion into a Ni−H

https://dx.doi.org/10.1021/jacs.0c00905
J. Am. Chem. Soc. 2020, 142, 5396−5407

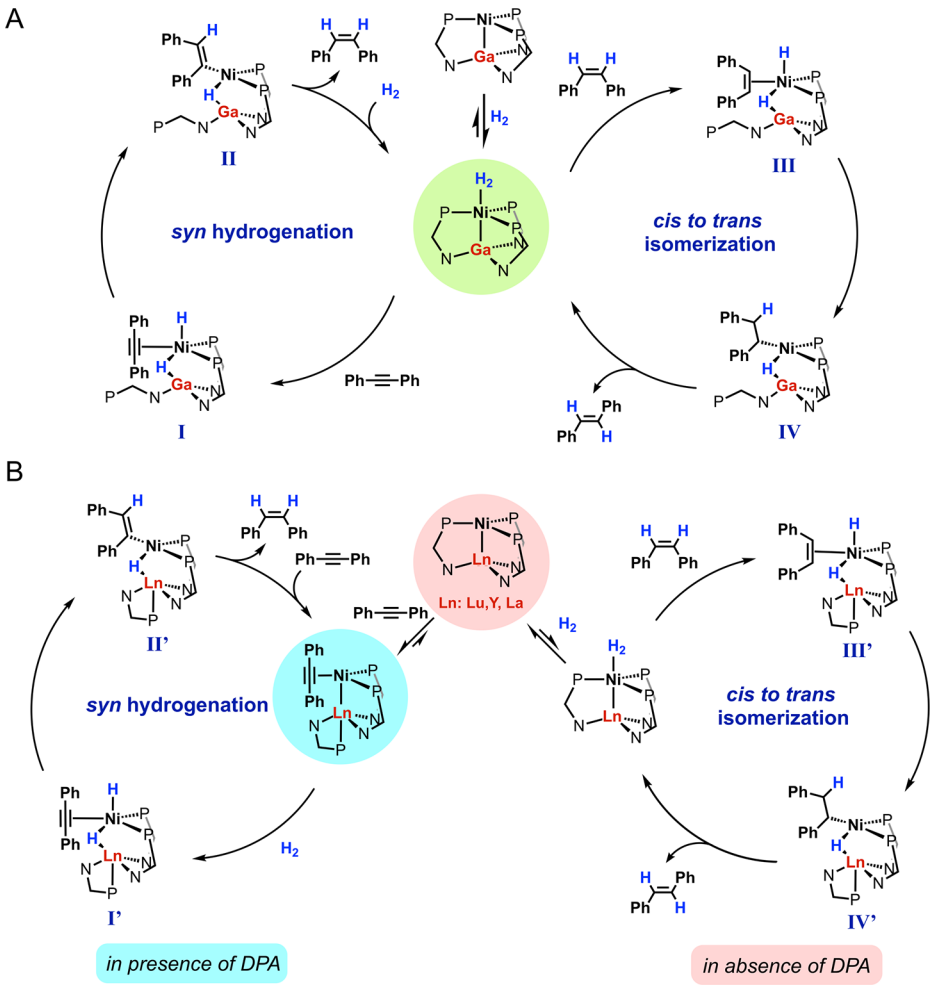

Figure 6. Proposed catalytic cycles for the nickel-catalyzed (*E*)-selective semihydrogenation of diphenylacetylene: (A) Ni−Ga and (B) Ni−Ln.

bond and subsequent C−C bond rotation and *β*-hydride elimination.

DISCUSSION

The mechanistic and kinetic studies provide a comprehensive understanding of how the choice of the M(III) support impacts the Ni−M semihydrogenation catalysis. Both the size and the Lewis acidity of the M(III) ion play significant roles. The larger M(III) ions with an ionic radius ≥0.86 Å all favor a catalyst resting state of the alkyne adduct, Ni(η^2-PhC≡CPh), during the first catalytic cycle. This subgroup includes the Ni−Ln catalysts, where M is Lu, Y, and La. During the second catalytic cycle when DPA is depleted, these catalysts change their resting state to the "naked" species, $NiML_3$, which suggests that both alkene and H_2 binding are weak. Of note, the observation of the Ni(η^2-PhC≡CPh) catalyst resting state is directly coupled to the rare observation of a temporally separated autotandem catalysis, which to our knowledge has not been reported for alkyne semihydrogenation. Hence, the temporal separation is a direct consequence of the nearly perfect chemoselectivity of the Ni−Ln catalysts for reacting with alkynes over alkenes when both substrates are present.

The Lewis acidity of the M(III) support can influence both the catalyst resting state and the catalytic rates. The H_2 adduct resting state, Ni(η^2-H_2), is only observed for Ni−Ga **9**. Previously, increasingly electron-deficient Ni(0) centers were shown to bind H_2 more strongly.[39,71] The observation of **9**-H_2 as the resting state in both catalytic cycles follows a similar logic in that Ga(III), which is by far the most Lewis acidic ion in this series, would withdraw the most Ni electron density. Catalyst **9** further stands out for its fastest initial rates in (*Z*)-stilbene isomerization in the series, by nearly 2 orders of magnitude. Even among the remaining Ni−RE catalysts, the *more* Lewis acidic RE ions promote *faster* (*Z*)-stilbene isomerization (Figure 3). By contrast, the *more* Lewis acidic RE ions yield *slower* initial rates in the *syn*-hydrogenation of DPA. We posit that alkyne binding is favored by a more electron-rich Ni center, which can better *π*-back-bond to the alkyne. Furthermore, we propose that alkyne binding is more critical to the first catalytic cycle, whereas H_2 binding and activation play a more important role during the second catalytic cycle.

Figure 6 shows the proposed mechanism for the selective hydrogenation of DPA to (*E*)-stilbene. Since Ni−Ga **9** and the Ni−Ln (where Ln = Lu, Y, and La) complexes feature different catalyst resting states, their mechanisms are shown separately. The Ni−Ga catalyst first binds H_2 to generate **9**−H_2, the observed resting state. Activation of H_2, followed by phosphine dissociation[35] and then DPA binding,[80−82] leads to the formation of intermediate **I**. The bridging and terminal hydrides, HNi(*μ*−H)Ga, in **I** are based on the analogous HNi(*μ*−H)B species reported by Peters,[28,83] as well as Thomas' HCo(*μ*−H)Zr intermediate.[59] We note that the mechanistic data does not discern whether alkyne binding or

https://dx.doi.org/10.1021/jacs.0c00905
J. Am. Chem. Soc. 2020, 142, 5396−5407

H−H cleavage proceeds first in the cycle. Next, migratory insertion of the alkyne into the Ni−H bond forms the Ni vinyl intermediate, **II**. The first catalytic cycle ends with the reductive elimination of (*Z*)-stilbene and binding of H_2 to regenerate **9**−H_2. In the second catalytic cycle, H_2 activation, followed by phosphine dissociation to allow for (*Z*)-stilbene binding, would provide intermediate **III**, which is the alkene counterpart to **I**. Migratory insertion of the alkene into the Ni−H generates the Ni diphenylethyl intermediate **IV**. Rotation of the ethyl C−C bond followed by *β*-hydride elimination would generate (*E*)-stilbene, as supported by the isotope labeling studies described above. Alternatively, from **IV**, reductive elimination may proceed to form the 1,2-diphenylethane byproduct.

The Ni−Ln catalysts are proposed to operate through similar intermediates, **I′**−**IV′**, though their mechanism diverges in key ways. First, by favoring DPA binding, the Ni−Ln catalysts operate via the Ni(η^2-PhC≡CPh) resting state, wherein the dissociated phosphine binds to the Ln ion. Second, owing to the favorability of the alkyne adduct, (*Z*)-stilbene cannot enter the *cis*-to-*trans* isomerization cycle until nearly all the DPA is depleted, and Ni(η^2-PhC≡CPh) is no longer the default resting state. The isomerization cycle is similar to that described above for Ni−Ga **9**, except that the "naked" $NiLnL_3$ species is the new resting state. Likewise, H_2 binding is proposed to precede alkene binding since the $NiLnL_3$ complexes all exhibit weak binding of H_2, whereas alkene binding has not yet been detected for any of these catalysts.

For Ni−Sc **6**, the catalyst resting state throughout the full catalysis is $NiScL_3$. Presumably, the Sc(III) support is neither sufficiently large (0.75 Å) to accommodate a stable Ni(η^2-PhC≡CPh) adduct nor particularly Lewis acidic (pK_a 5.1) to promote strong H_2 binding at Ni. The Ni−Sc **6** showed the slowest initial rate in the *syn*-hydrogenation of DPA, which hinders its performance in the overall catalysis. Moreover, Ni−Sc generates the highest percentage of the (*Z*,*Z*)-diene byproduct (15%) in the series. The formation of the *Z*,*Z*-diene points to an alternative path whereby migratory insertion of DPA into the Ni vinyl bond in intermediate **II** occurs prior to reductive elimination.

CONCLUSION

The Ni−rare earth complexes add to the few first-row transition metal−rare earth complexes with direct metal−metal bonding interactions. More significantly, this study demonstrates the utility of rare earth metal ions as promoters in base-metal catalysis. Both the ionic size and Lewis acidity of the metal support are important tunable parameters for the catalytic activity and selectivity. First, the Ni electronics are significantly perturbed by variation of the M(III) support: the Ni(I/0) peak potentials were tuned overall by 0.75 V and showed a strong correlation with M(III) Lewis acidity. Second, the M(III) support can remotely tune the substrate-binding preference of the active Ni center and, consequently, determine the catalyst resting state. The weak Lewis acidity and the large ionic size of the rare-earth supports are posited to be responsible for the strong Ni-alkyne binding in Ni−Y **7**, Ni−Lu **1**, and Ni−La **8**. Presumably, these more electron-rich Ni centers can better *π*-back-bond into the alkyne unit, while the large rare-earth supports provide an intramolecular, open coordination site to favor hemilability of the phosphine ligand. On the other hand, strong Lewis acidity appears to be the dominant parameter in priming Ni for strong H_2 binding as only the highly Lewis acidic Ga(III) formed a stable Ni(η^2-H_2) adduct under ambient conditions. The delineation of size and Lewis acidity in determining substrate binding is corroborated by the fact that Ni−Sc **6**, which falls in the middle in terms of both Lewis acidity and size, showed neither alkyne nor H_2 binding under ambient conditions.

The stark differences in substrate binding among the Ni−M catalysts have important mechanistic and kinetic ramifications. When the Ni−M complex binds alkyne strongly, the ensuing autotandem catalysis shows a clear temporal separation between the two catalytic cycles. This separation also indicates a stronger chemoselectivity for alkyne over alkene reactivity. Similarly, for the Ni-rare earth catalysts, the rate of DPA *syn*-hydrogenation appears to be directly influenced by its ability to bind alkyne, such that *less* Lewis acidic rare-earth ions yield faster initial rates in the *syn*-hydrogenation of DPA. The opposite trend was found for the rate of alkene isomerization, where *more* Lewis acidic rare-earth ions yield faster initial rates. This may suggest that H_2 binding and activation are dependent on the Lewis acidity of the support and are the critical step in alkene isomerization for these catalysts.

ASSOCIATED CONTENT

Supporting Information

The Supporting Information is available free of charge at https://pubs.acs.org/doi/10.1021/jacs.0c00905.

X-ray crystallographic data for complexes **2**−**9**, **7**−THF, **7**−DPA, and **8′** (CIF)

Experimental procedures, characterization, and spectroscopic data (PDF)

AUTHOR INFORMATION

Corresponding Author

Connie C. Lu − *Department of Chemistry, University of Minnesota, Minneapolis, Minnesota 55455-0431, United States;* orcid.org/0000-0002-5162-9250; Email: clu@umn.edu

Author

Bianca L. Ramirez − *Department of Chemistry, University of Minnesota, Minneapolis, Minnesota 55455-0431, United States*

Complete contact information is available at: https://pubs.acs.org/10.1021/jacs.0c00905

Notes

The authors declare no competing financial interest.

The cif files for complexes **2**−**9**, **7**−THF, **7**−DPA, and **8′** have been deposited in the Cambridge CCDC as nos.1979220−1979230.

ACKNOWLEDGMENTS

B.L.R. is grateful to 3M for a research fellowship. The experimental work was supported by the American Chemical Society Petroleum Research Fund (57192-ND3). C.C.L. acknowledges the National Science Foundation (CHE-1665010 and CHE-1954751) for support. X-ray diffraction experiments were performed using a crystal diffractometer acquired through an NSF-MRI award (CHE-1229400) in the X-ray laboratory supervised by Dr. Victor G. Young, Jr. B.L.R. thanks Dr. Victor G. Young, Jr. for assistance with X-ray

crystallography and Dr. Letitia J. Yao for assistance with NMR spectroscopy.

REFERENCES

(1) Liddle, S. T.; Mills, D. P. Metal-metal bonds in f-element chemistry. *Dalton Trans.* **2009**, 5592−5605.

(2) Butovskii, M. V.; Kempe, R. Rare earth−metal bonding in molecular compounds: recent advances, challenges, and perspectives. *New J. Chem.* **2015**, *39*, 7544−7558.

(3) Oelkers, B.; Kempe, R., Group 3, Lanthanide, and Actinide Metal−Metal Bonds. In *Molecular Metal-Metal Bonds*, 1st ed.; Liddle, S. T., Ed.; Wiley-VCH Verlag GmbH & Co. KGaA: Weinheim, 2015; pp 47−71, DOI: 10.1002/9783527673353.ch3.

(4) Spannenberg, A.; Oberthür, M.; Noss, H.; Tillack, A.; Arndt, P.; Kempe, R. Metal—Metal "Communication" of Rh or Pd with Nd in Novel Heterobinuclear Complexes. *Angew. Chem., Int. Ed.* **1998**, *37*, 2079−2082.

(5) Butovskii, M. V.; Tok, O. L.; Wagner, F. R.; Kempe, R. Bismetallocenes: Lanthanoid−Transition-Metal Bonds through Alkane Elimination. *Angew. Chem., Int. Ed.* **2008**, *47*, 6469−6472.

(6) Shima, T.; Hou, Z. Activation and Dehydrogenative Silylation of the C−H Bonds of Phosphine-coordinated Ruthenium in Lu/Ru Heteromultimetallic Hydride Complexes. *Chem. Lett.* **2008**, *37*, 298−299.

(7) Döring, C.; Dietel, A. M.; Butovskii, M. V.; Bezugly, V.; Wagner, F. R.; Kempe, R. Molecular $[Yb(TM)_2]$ Intermetalloids (TM = Ru, Re). *Chem. - Eur. J.* **2010**, *16*, 10679−10683.

(8) Nakajima, Y.; Hou, Z. Rare-Earth-Metal/Platinum Heterobinuclear Complexes Containing Reactive Ln-alkyl groups (Ln = Y, Lu): Synthesis, Structural Characterization, and Reactivity. *Organometallics* **2009**, *28*, 6861−6870.

(9) Arnold, P. L.; McMaster, J.; Liddle, S. T. An unsupported transition metal-lanthanide bond; synthesis and crystal structure of an Nd-Fe amido N-heterocyclic carbene complex. *Chem. Commun.* **2009**, 818−820.

(10) O, W. W. N.; Kang, X.; Luo, Y.; Hou, Z. PNP-Ligated Heterometallic Rare-Earth/Ruthenium Hydride Complexes Bearing Phosphinophenyl and Phosphinomethyl Bridging Ligands. *Organometallics* **2014**, *33*, 1030−1043.

(11) Völcker, F.; Mück, F. M.; Vogiatzis, K. D.; Fink, K.; Roesky, P. W. Bi- and trimetallic rare-earth-palladium complexes ligated by phosphinoamides. *Chem. Commun.* **2015**, *51*, 11761−11764.

(12) Völcker, F.; Roesky, P. W. Bimetallic rare-earth/platinum complexes ligated by phosphinoamides. *Dalton Trans.* **2016**, *45*, 9429−9435.

(13) Cui, P.; Xiong, C.; Du, J.; Huang, Z.; Xie, S.; Wang, H.; Zhou, S.; Fang, H.; Wang, S. Heterobimetallic scandium−group 10 metal complexes with LM → Sc (LM = Ni, Pd, Pt) dative bonds. *Dalton Trans.* **2020**, *49*, 124−130.

(14) Du, J.; Huang, Z.; Zhang, Y.; Wang, S.; Zhou, S.; Fang, H.; Cui, P. A Scandium Metalloligand-Based Heterobimetallic Pd−Sc Complex: Electronic Tuning Through a Very Short Pd→Sc Dative Bond. *Chem. - Eur. J.* **2019**, *25*, 10149−10155.

(15) Burns, C. P.; Yang, X.; Sung, S.; Wofford, J. D.; Bhuvanesh, N. S.; Hall, M. B.; Nippe, M. Towards understanding of lanthanide−transition metal bonding: investigations of the first Ce−Fe bonded complex. *Chem. Commun.* **2018**, *54*, 10893−10896.

(16) Burns, C. P.; Yang, X.; Wofford, J. D.; Bhuvanesh, N. S.; Hall, M. B.; Nippe, M. Structure and Magnetization Dynamics of Dy−Fe and Dy−Ru Bonded Complexes. *Angew. Chem., Int. Ed.* **2018**, *57*, 8144−8148.

(17) (a) Schwob, T.; Kunnas, P.; de Jonge, N.; Papp, C.; Steinrück, H.-P.; Kempe, R. General and selective deoxygenation by hydrogen using a reusable earth-abundant metal catalyst. *Sci. Adv.* **2019**, *5*, No. eaav3680. (b) Bruix, A.; Rodriguez, J. A.; Ramírez, P. J.; Senanayake, S. D.; Evans, J.; Park, J. B.; Stacchiola, D.; Liu, P.; Hrbek, J.; Illas, F. A New Type of Strong Metal−Support Interaction and the Production of H_2 through the Transformation of Water on Pt/CeO_2(111) and Pt/CeO_x/TiO_2(110) Catalysts. *J. Am. Chem. Soc.* **2012**, *134*, 8968−8974.

(18) Ahmadi, M.; Mistry, H.; Roldan Cuenya, B. Tailoring the Catalytic Properties of Metal Nanoparticles via Support Interactions. *J. Phys. Chem. Lett.* **2016**, *7*, 3519−3533.

(19) Evangelisti, F.; Moré, R.; Hodel, F.; Luber, S.; Patzke, G. R. 3d−4f $\{Co^{II}_3Ln(OR)_4\}$ Cubanes as Bio-Inspired Water Oxidation Catalysts. *J. Am. Chem. Soc.* **2015**, *137*, 11076−11084.

(20) Hodel, F. H.; Luber, S. Redox-Inert Cations Enhancing Water Oxidation Activity: The Crucial Role of Flexibility. *ACS Catal.* **2016**, *6*, 6750−6761.

(21) Kumar, P.; Griffiths, K.; Anson, C. E.; Powell, A. K.; Kostakis, G. E. A tetranuclear $Cu^{II}_2Dy^{III}_2$ coordination cluster as a Suzuki (C−C) coupling reaction promoter. *Dalton Trans.* **2018**, *47*, 17202−17205.

(22) Sai Manoj Gorantla, N. V. T.; Guruprasad Reddy, P.; Abdul Shakoor, S. M.; Mandal, R.; Roy, S.; Mondal, K. C. Tetranuclear 3d/4f Coordination Complexes as Homogeneous Catalysts for Bis-(indolyl)methane Syntheses. *ChemistrySelect* **2019**, *4*, 7722−7727.

(23) Broderick, E. M.; Diaconescu, P. L. Cerium(IV) Catalysts for the Ring-Opening Polymerization of Lactide. *Inorg. Chem.* **2009**, *48*, 4701−4706.

(24) Broderick, E. M.; Guo, N.; Wu, T.; Vogel, C. S.; Xu, C.; Sutter, J.; Miller, J. T.; Meyer, K.; Cantat, T.; Diaconescu, P. L. Redox control of a polymerization catalyst by changing the oxidation state of the metal center. *Chem. Commun.* **2011**, *47*, 9897−9899.

(25) Wang, X.; Brosmer, J. L.; Thevenon, A.; Diaconescu, P. L. Highly Active Yttrium Catalysts for the Ring-Opening Polymerization of ϵ-Caprolactone and δ-Valerolactone. *Organometallics* **2015**, *34*, 4700−4706.

(26) Amgoune, A.; Bourissou, D. σ-Acceptor, Z-type ligands for transition metals. *Chem. Commun.* **2011**, *47*, 859−871.

(27) Buchwalter, P.; Rosé, J.; Braunstein, P. Multimetallic Catalysis Based on Heterometallic Complexes and Clusters. *Chem. Rev.* **2015**, *115*, 28−126.

(28) Harman, W. H.; Lin, T.-P.; Peters, J. C. A d^{10} Ni−(H_2) Adduct as an Intermediate in H−H Oxidative Addition across a Ni−B Bond. *Angew. Chem., Int. Ed.* **2014**, *53*, 1081−1086.

(29) Mankad, N. P. Selectivity Effects in Bimetallic Catalysis. *Chem. - Eur. J.* **2016**, *22*, 5822−5829.

(30) Bouhadir, G.; Bourissou, D. Complexes of ambiphilic ligands: reactivity and catalytic applications. *Chem. Soc. Rev.* **2016**, *45*, 1065−1079.

(31) Powers, I. G.; Uyeda, C. Metal−Metal Bonds in Catalysis. *ACS Catal.* **2017**, *7*, 936−958.

(32) Pye, D. R.; Mankad, N. P. Bimetallic catalysis for C−C and C−X coupling reactions. *Chem. Sci.* **2017**, *8*, 1705−1718.

(33) Thomas, C. M. Metal-Metal Multiple Bonds in Early/Late Heterobimetallic Complexes: Applications Toward Small Molecule Activation and Catalysis. *Comments Inorg. Chem.* **2011**, *32*, 14−38.

(34) You, D.; Gabbaï, F. P. Unmasking the Catalytic Activity of a Platinum Complex with a Lewis Acidic, Non-innocent Antimony Ligand. *J. Am. Chem. Soc.* **2017**, *139*, 6843−6846.

(35) Cammarota, R. C.; Clouston, L. J.; Lu, C. C. Leveraging molecular metal−support interactions for H_2 and N_2 activation. *Coord. Chem. Rev.* **2017**, *334*, 100−111.

(36) Sircoglou, M.; Bontemps, S.; Bouhadir, G.; Saffon, N.; Miqueu, K.; Gu, W.; Mercy, M.; Chen, C.-H.; Foxman, B. M.; Maron, L.; Ozerov, O. V.; Bourissou, D. Group 10 and 11 Metal Boratranes (Ni, Pd, Pt, CuCl, AgCl, AuCl, and Au^+) Derived from a Triphosphine−Borane. *J. Am. Chem. Soc.* **2008**, *130*, 16729−16738.

(37) Takaya, J.; Iwasawa, N. Synthesis, Structure, and Catalysis of Palladium Complexes Bearing a Group 13 Metalloligand: Remarkable Effect of an Aluminum-Metalloligand in Hydrosilylation of CO_2. *J. Am. Chem. Soc.* **2017**, *139*, 6074−6077.

(38) You, D.; Gabbaï, F. P. Tunable σ-Accepting, Z-Type Ligands for Organometallic Catalysis. *Trends in Chemistry* **2019**, *1*, 485−496.

https://dx.doi.org/10.1021/jacs.0c00905
J. Am. Chem. Soc. 2020, 142, 5396−5407

(39) Cammarota, R. C.; Lu, C. C. Tuning Nickel with Lewis Acidic Group 13 Metalloligands for Catalytic Olefin Hydrogenation. *J. Am. Chem. Soc.* **2015**, *137*, 12486−12489.
(40) Cammarota, R. C.; Vollmer, M. V.; Xie, J.; Ye, J.; Linehan, J. C.; Burgess, S. A.; Appel, A. M.; Gagliardi, L.; Lu, C. C. A Bimetallic Nickel−Gallium Complex Catalyzes CO_2 Hydrogenation via the Intermediacy of an Anionic d^{10} Nickel Hydride. *J. Am. Chem. Soc.* **2017**, *139*, 14244−14250.
(41) Ramirez, B. L.; Sharma, P.; Eisenhart, R. J.; Gagliardi, L.; Lu, C. C. Bimetallic nickel-lutetium complexes: tuning the properties and catalytic hydrogenation activity of the Ni site by varying the Lu coordination environment. *Chem. Sci.* **2019**, *10*, 3375−3384.
(42) Crespo-Quesada, M.; Cárdenas-Lizana, F.; Dessimoz, A.-L.; Kiwi-Minsker, L. Modern Trends in Catalyst and Process Design for Alkyne Hydrogenations. *ACS Catal.* **2012**, *2*, 1773−1786.
(43) de Vries, J. G.; Elsevier, C. J., Eds.; *The Handbook of Homogeneous Hydrogenation*; Weinheim: Wiley-VCH, 2007; DOI: 10.1002/9783527619382.
(44) Swamy, K. C. K.; Reddy, A. S.; Sandeep, K.; Kalyani, A. Advances in chemoselective and/or stereoselective semihydrogenation of alkynes. *Tetrahedron Lett.* **2018**, *59*, 419−429.
(45) Lindlar, H.; Dubuis, R. Palladium Catalyst for the Partial Reduction of Acetylenes. *Org. Synth.* **1966**, *46*, 89.
(46) Schrock, R. R.; Osborn, J. A. Catalytic hydrogenation using cationic rhodium complexes. II. The selective hydrogenation of alkynes to cis olefins. *J. Am. Chem. Soc.* **1976**, *98*, 2143−2147.
(47) van Laren, M. W.; Elsevier, C. J. Selective Homogeneous Palladium(0)-Catalyzed Hydrogenation of Alkynes to (Z)-Alkenes. *Angew. Chem., Int. Ed.* **1999**, *38*, 3715−3717.
(48) Gianetti, T. L.; Tomson, N. C.; Arnold, J.; Bergman, R. G. Z-Selective, Catalytic Internal Alkyne Semihydrogenation under H_2/CO Mixtures by a Niobium(III) Imido Complex. *J. Am. Chem. Soc.* **2011**, *133*, 14904−14907.
(49) La Pierre, H. S.; Arnold, J.; Toste, F. D. Z-Selective Semihydrogenation of Alkynes Catalyzed by a Cationic Vanadium Bisimido Complex. *Angew. Chem., Int. Ed.* **2011**, *50*, 3900−3903.
(50) Tseng, K.-N. T.; Kampf, J. W.; Szymczak, N. K. Modular Attachment of Appended Boron Lewis Acids to a Ruthenium Pincer Catalyst: Metal−Ligand Cooperativity Enables Selective Alkyne Hydrogenation. *J. Am. Chem. Soc.* **2016**, *138*, 10378−10381.
(51) Gorgas, N.; Brünig, J.; Stöger, B.; Vanicek, S.; Tilset, M.; Veiros, L. F.; Kirchner, K. Efficient Z-Selective Semihydrogenation of Internal Alkynes Catalyzed by Cationic Iron(II) Hydride Complexes. *J. Am. Chem. Soc.* **2019**, *141*, 17452−17458.
(52) Fürstner, A. trans-Hydrogenation, gem-Hydrogenation, and trans-Hydrometalation of Alkynes: An Interim Report on an Unorthodox Reactivity Paradigm. *J. Am. Chem. Soc.* **2019**, *141*, 11−24.
(53) Leutzsch, M.; Wolf, L. M.; Gupta, P.; Fuchs, M.; Thiel, W.; Farès, C.; Fürstner, A. Formation of Ruthenium Carbenes by gem-Hydrogen Transfer to Internal Alkynes: Implications for Alkyne trans-Hydrogenation. *Angew. Chem., Int. Ed.* **2015**, *54*, 12431−12436.
(54) Guthertz, A.; Leutzsch, M.; Wolf, L. M.; Gupta, P.; Rummelt, S. M.; Goddard, R.; Farès, C.; Thiel, W.; Fürstner, A. Half-Sandwich Ruthenium Carbene Complexes Link trans-Hydrogenation and gem-Hydrogenation of Internal Alkynes. *J. Am. Chem. Soc.* **2018**, *140*, 3156−3169.
(55) Radkowski, K.; Sundararaju, B.; Fürstner, A. A Functional-Group-Tolerant Catalytic trans Hydrogenation of Alkynes. *Angew. Chem., Int. Ed.* **2013**, *52*, 355−360.
(56) Schleyer, D.; Niessen, H. G.; Bargon, J. In situ ^{1}H-PHIP-NMR studies of the stereoselective hydrogenation of alkynes to (E)-alkenes catalyzed by a homogeneous $[Cp^*Ru]^+$ catalyst. *New J. Chem.* **2001**, *25*, 423−426.
(57) Srimani, D.; Diskin-Posner, Y.; Ben-David, Y.; Milstein, D. Iron Pincer Complex Catalyzed, Environmentally Benign, E-Selective Semi-Hydrogenation of Alkynes. *Angew. Chem., Int. Ed.* **2013**, *52*, 14131−14134.
(58) Tokmic, K.; Fout, A. R. Alkyne Semihydrogenation with a Well-Defined Nonclassical Co−H_2 Catalyst: A H_2 Spin on Isomerization and E-Selectivity. *J. Am. Chem. Soc.* **2016**, *138*, 13700−13705.
(59) Gramigna, K. M.; Dickie, D. A.; Foxman, B. M.; Thomas, C. M. Cooperative H_2 Activation across a Metal−Metal Multiple Bond and Hydrogenation Reactions Catalyzed by a Zr/Co Heterobimetallic Complex. *ACS Catal.* **2019**, *9*, 3153−3164.
(60) Murugesan, K.; Bheeter, C. B.; Linnebank, P. R.; Spannenberg, A.; Reek, J. N. H.; Jagadeesh, R. V.; Beller, M. Nickel-Catalyzed Stereodivergent Synthesis of *E*- and *Z*-Alkenes by Hydrogenation of Alkynes. *ChemSusChem* **2019**, *12*, 3363−3369.
(61) Karunananda, M. K.; Mankad, N. P. *E*-Selective Semi-Hydrogenation of Alkynes by Heterobimetallic Catalysis. *J. Am. Chem. Soc.* **2015**, *137*, 14598−14601.
(62) Karunananda, M. K.; Mankad, N. P. Heterobimetallic H_2 Addition and Alkene/Alkane Elimination Reactions Related to the Mechanism of E-Selective Alkyne Semihydrogenation. *Organometallics* **2017**, *36*, 220−227.
(63) Muhammad, S. R.; Nugent, J. W.; Tokmic, K.; Zhu, L.; Mahmoud, J.; Fout, A. R. Electronic Ligand Modifications on Cobalt Complexes and Their Application toward the Semi-Hydrogenation of Alkynes and Para-Hydrogenation of Alkenes. *Organometallics* **2019**, *38*, 3132−3138.
(64) Higashida, K.; Mashima, K. E-Selective Semi-hydrogenation of Alkynes with Dinuclear Iridium Complexes under Atmospheric Pressure of Hydrogen. *Chem. Lett.* **2016**, *45*, 866−868.
(65) Chirik, P.; Morris, R. Getting Down to Earth: The Renaissance of Catalysis with Abundant Metals. *Acc. Chem. Res.* **2015**, *48*, 2495−2495.
(66) White, M. C. Base-Metal Catalysis: Embrace the Wild Side. *Adv. Synth. Catal.* **2016**, *358*, 2364−2365.
(67) Herbert, D. E.; Lionetti, D.; Rittle, J.; Agapie, T. Heterometallic Triiron-Oxo/Hydroxo Clusters: Effect of Redox-Inactive Metals. *J. Am. Chem. Soc.* **2013**, *135*, 19075−19078.
(68) Lin, P.-H.; Takase, M. K.; Agapie, T. Investigations of the Effect of the Non-Manganese Metal in Heterometallic-Oxido Cluster Models of the Oxygen Evolving Complex of Photosystem II: Lanthanides as Substitutes for Calcium. *Inorg. Chem.* **2015**, *54*, 59−64.
(69) Tsui, E. Y.; Agapie, T. Reduction potentials of heterometallic manganese−oxido cubane complexes modulated by redox-inactive metals. *Proc. Natl. Acad. Sci. U. S. A.* **2013**, *110*, 10084−10088.
(70) Tsui, E. Y.; Tran, R.; Yano, J.; Agapie, T. Redox-inactive metals modulate the reduction potential in heterometallic manganese−oxido clusters. *Nat. Chem.* **2013**, *5*, 293.
(71) Cammarota, R. C.; Xie, J.; Burgess, S. A.; Vollmer, M. V.; Vogiatzis, K. D.; Ye, J.; Linehan, J. C.; Appel, A. M.; Hoffmann, C.; Wang, X.; Young, V. G.; Lu, C. C. Thermodynamic and kinetic studies of H_2 and N_2 binding to bimetallic nickel-group 13 complexes and neutron structure of a Ni(η^2-H_2) adduct. *Chem. Sci.* **2019**, *10*, 7029−7042.
(72) Shannon, R. Revised effective ionic radii and systematic studies of interatomic distances in halides and chalcogenides. *Acta Crystallogr., Sect. A* **1976**, *32*, 751−767.
(73) Pyykkö, P. Additive Covalent Radii for Single-, Double-, and Triple-Bonded Molecules and Tetrahedrally Bonded Crystals: A Summary. *J. Phys. Chem. A* **2015**, *119*, 2326−2337.
(74) Li, L.; Herzon, S. B. Temporal separation of catalytic activities allows anti-Markovnikov reductive functionalization of terminal alkynes. *Nat. Chem.* **2014**, *6*, 22−27.
(75) Kaeffer, N.; Larmier, K.; Fedorov, A.; Copéret, C. Origin of ligand-driven selectivity in alkyne semihydrogenation over silica-supported copper nanoparticles. *J. Catal.* **2018**, *364*, 437−445.
(76) Desrosiers, P. J.; Cai, L.; Lin, Z.; Richards, R.; Halpern, J. Assessment of the "T_1 criterion" for distinguishing between classical and nonclassical transition-metal hydrides: hydride relaxation rates in tris(triarylphosphine)osmium tetrahydrides and related polyhydrides. *J. Am. Chem. Soc.* **1991**, *113*, 4173−4184.

https://dx.doi.org/10.1021/jacs.0c00905
J. Am. Chem. Soc. 2020, 142, 5396−5407

(77) Luther, T. A.; Heinekey, D. M. Synthesis, Characterization, and Reactivity of Dicationic Dihydrogen Complexes of Osmium and Ruthenium. *Inorg. Chem.* **1998**, *37*, 127−132.
(78) Thomas, C. M.; Napoline, J. W.; Rowe, G. T.; Foxman, B. M. Oxidative addition across Zr/Co multiple bonds in early/late heterobimetallic complexes. *Chem. Commun.* **2010**, *46*, 5790−5792.
(79) Zhang, H.; Wu, B.; Marquard, S. L.; Litle, E. D.; Dickie, D. A.; Bezpalko, M. W.; Foxman, B. M.; Thomas, C. M. Investigation of Ketone C═O Bond Activation Processes by Heterobimetallic Zr/Co and Ti/Co Tris(phosphinoamide) Complexes. *Organometallics* **2017**, *36*, 3498−3507.
(80) Bianchini, C.; Meli, A.; Peruzzini, M.; Frediani, P.; Bohanna, C.; Esteruelas, M. A.; Oro, L. A. Selective hydrogenation of 1-alkynes to alkenes catalyzed by an iron(II) cis-hydride η^2-dihydrogen complex. A case of intramolecular reaction between η^2-H_2 and sigma-vinyl ligands. *Organometallics* **1992**, *11*, 138−145.
(81) Bianchini, C.; Meli, A.; Peruzzini, M.; Vizza, F.; Zanobini, F.; Frediani, P. A homogeneous iron(II) system capable of selectivity catalyzing the reduction of terminal alkynes to alkenes and buta-1,3-dienes. *Organometallics* **1989**, *8*, 2080−2082.
(82) Kubas, G. J. Fundamentals of H_2 Binding and Reactivity on Transition Metals Underlying Hydrogenase Function and H_2 Production and Storage. *Chem. Rev.* **2007**, *107*, 4152−4205.
(83) Harman, W. H.; Peters, J. C. Reversible H_2 Addition across a Nickel−Borane Unit as a Promising Strategy for Catalysis. *J. Am. Chem. Soc.* **2012**, *134*, 5080−5082.

https://dx.doi.org/10.1021/jacs.0c00905
J. Am. Chem. Soc. 2020, 142, 5396−5407